Joule

CellPress

Article

Realization of High Thermoelectric Figure of Merit in GeTe by Complementary Co-doping of Bi and In

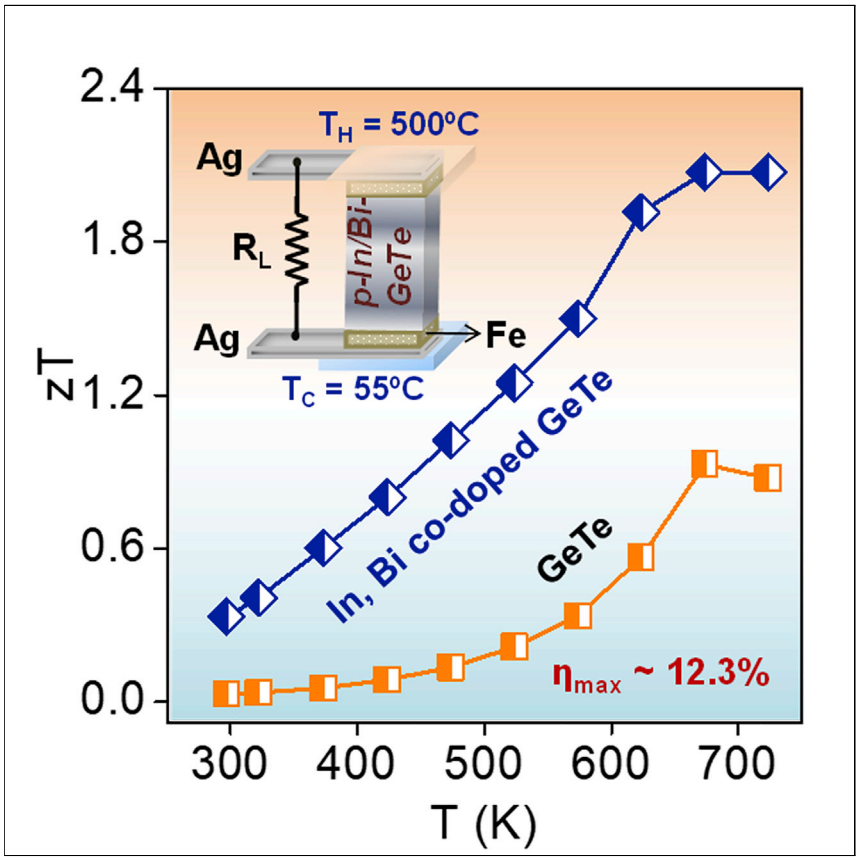

Synergistic effect of In-induced resonance level and Bi-induced point defect phonon scattering resulted in high thermoelectric figure of merit, zT ~ 2.1 at 723 K in In and Bi co-doped GeTe along with extremely high thermoelectric power conversion efficiency, η ~ 12.3% in single-leg thermoelectric generator for the temperature difference of 445 K.

Suresh Perumal, Manisha Samanta, Tanmoy Ghosh, ..., Ajay Singh, Umesh V. Waghmare, Kanishka Biswas

kanishka@jncasr.ac.in

HIGHLIGHTS

In doping boosts the Seebeck coefficient of GeTe by creating resonance level

Bi-doping-induced point defects and domain variants decrease κ_{lat} of GeTe

In and Bi co-doped GeTe shows a high thermoelectric figure of merit zT of ~2.1 at 723 K

Single-leg TE device of In, Bi co-doped GeTe has ~12.3% efficiency for a ΔT of ~445 K

Perumal et al., Joule 3, 2565–2580
October 16, 2019
https://doi.org/10.1016/j.joule.2019.08.017

Joule

CellPress

Article

Realization of High Thermoelectric Figure of Merit in GeTe by Complementary Co-doping of Bi and In

Suresh Perumal,[1,5,6] Manisha Samanta,[1,6] Tanmoy Ghosh,[1] U. Sandhya Shenoy,[2] Anil K. Bohra,[3] Shovit Bhattacharya,[3] Ajay Singh,[3] Umesh V. Waghmare,[2,4] and Kanishka Biswas[1,4,7,*]

SUMMARY

GeTe and its derivatives have recently attracted wide attention as promising thermoelectric materials. The principle challenge in optimizing the thermoelectric figure of merit, *zT*, is the low Seebeck coefficient (*S*) and high thermal conductivity of GeTe. Here, we report a high *zT* of ~2.1 at 723 K in In and Bi co-doped GeTe along with an extremely high TE conversion efficiency of ~12.3% in a single-leg thermoelectric generator for the temperature difference of 445 K. In and Bi play a distinct but complementary role. In doping significantly enhances the *S* through the formation of resonance level, which is confirmed with first-principles density functional theory calculations and Pisarenko plot considering two valance band model. However, Bi doping markedly reduces the lattice thermal conductivity due to the formation of extensive solid solution point defects and domain variants. Moreover, a high value of Vickers microhardness (~200 H_v, H_v = kgf/mm^2) reveals excellent mechanical stability.

INTRODUCTION

Thermoelectric (TE) materials have recently drawn great attention to materials research for thermal energy management and utilization because of their ability to directly convert waste heat into electricity without emitting toxic gases and without involving moving parts.[1–3] The power conversion efficiency (η) of TE materials is directly related to Carnot efficiency ($\eta_C = T_H - T_C/T_H$, where T_H is the temperature of heat source, and T_C is the temperature of heat sink) and the TE figure of merit, $zT = S^2\sigma T/\kappa_{total}$, where, S, σ, κ_{total}, and T are the Seebeck coefficient, electrical conductivity, total thermal conductivity, and absolute temperature, respectively.[1–3] Notable attempts to develop materials with high zT generally involves a reduction of lattice thermal conductivity (κ_{lat}) via phonon scattering by solid solution point defects,[4–6] hierarchical nano- and meso-scale architectures[7,8] and other intrinsic factors,[9–13] and enhancing the Seebeck coefficient via electronic structure modulation.[14–18]

PbTe and its derivatives are well-known for their superior thermoelectric performance in the mid-temperature operational range of 600–900 K.[7,14,17,18] However, the toxicity of Pb limits their large-scale applications necessitating the research for alternative thermoelectric materials. Although GeTe-based thermoelectric materials (such as TAGS-x) are known since the 1960s,[19,20] they have emerged as potential alternatives to PbTe only in recent years. Pristine GeTe contains intrinsic Ge vacancies, which causes excess *p*-type carrier density (~10^{21} cm^{-3}) that consequently results in a large σ of ~8,000 S/cm, low S of ~30 μV/K, and high κ_{total} of ~8 W/mK at 300 K with

Context & Scale

Thermoelectric (TE) materials are expected to play a prime role in future energy utilization and management. Pb-based materials have proven to be champion TE materials for mid-temperature power generation. However, the field demands Pb-free materials with high TE figure of merit (zT) along with high TE power conversion efficiency (η). Recently, GeTe has emerged as a potential alternative of PbTe. However, the low Seebeck coefficient and high thermal conductivity of GeTe are the two principle constraints in the way of optimizing its zT. Here, we have demonstrated a distinct but complementary role of In and Bi doping in GeTe in modulating the electronic structure and reducing the lattice thermal conductivity. These synergistic effects resulted in a high zT of ~2.1 at 723 K and an extremely high η of ~12.3% in single-leg TE generator for the temperature difference of 445 K in In and Bi co-doped GeTe. This co-doping approach with synergistic effects paves the way for the new generation of GeTe thermoelectrics.

a maximum zT of ~0.9 at 675 K.[21,22] Pristine GeTe undergoes second-order structural phase transition from high-temperature cubic (β-GeTe) to low-temperature rhombohedral (α-GeTe) phase at ~700 K due to thermal strain induced shift in Ge atoms during cooling from melt.[21–24] To enhance the Seebeck coefficient of GeTe, several intriguing methods have been employed recently, namely, sub-valence bands convergence,[25–30] slight symmetry reduction,[31,32] and formation of resonance states in the valence band.[33,34] Additionally, the lattice contribution to κ_{total} of GeTe has been significantly suppressed via nanostructuring[35–39] and solid solution alloying.[6,26,28,33,40,41] Although these state-of-the-art strategies have resulted in significant improvement in zT, the experimental power conversion efficiency (η), especially for the GeTe-based single-leg TE generator, has been limited in the range of 8%–9%.[42,43]

Substitution of Bi in GeTe is known to result in low $\kappa_{lat} \sim 1$ W/mK due to phonon scattering by solid solution point defects for Bi $\leq$ 6 mol %.[27,38,41] When Bi concentration is $\geq$10 mol %, the reduction of κ_{lat} is mainly attributed to the formation of nanoprecipitates and nanoscale cation defect layers.[38] Further, the aliovalent doping of Bi^{3+} at Ge^{2+} site in GeTe drastically reduces the p-type carrier density from ~10^{21} to ~10^{20} cm^{-3}.[27,38,41] On the other hand, the formation of resonant states close to Fermi level in the valence band of GeTe has been realized upon In doping,[33,34] which alters the density of states (DOS) near Fermi level leading to a significant enhancement in Seebeck coefficient. Therefore, In and Bi have different but complementary roles in the enhancement of the thermoelectric performance of GeTe. Thus, co-doping of In and Bi in GeTe may synergistically enhance the overall thermoelectric performance due to their complementary effects. Further, for practical applications, it is important to study the microhardness (mechanical stability) and investigate the experimental thermoelectric efficiency of single-leg TE devices based on high-performance Bi and In co-doped GeTe.

Herein, we demonstrate a significantly high thermoelectric performance in Bi and In co-doped GeTe, ascribed to distinct but complementary roles of In and Bi in terms of modulating the electronic structure and scattering of heat-carrying phonons, respectively. The enhanced Seebeck coefficient (~120 μV/K at 300 K) with In doping is shown to be due to the formation of resonance level in valence band and the reduced κ_{lat} (~0.5 W/mK at 300 K) is due to significant scattering of phonons at point defects associated with Bi substitution in GeTe. Their synergy results in a high thermoelectric figure of merit, zT, of 2.1 at 723 K and a high average TE figure of merit, zT_{avg}, of 1.3 in the temperature range of 300–723 K in the composition $Ge_{0.93}In_{0.01}Bi_{0.06}Te$. Fundamental understanding of the enhancement of Seebeck coefficient in In and Bi co-doped GeTe has been realized via first-principles density functional theoretical (DFT) calculations of electronic structure and Pisarenko plot considering two-band model, which reveals that In and Bi co-doping not only results in the formation of resonance level, it also facilitates the valence band convergence by decreasing the energy difference between the light and heavy hole valence bands. Further, the measured Vickers microhardness of the $Ge_{0.93}In_{0.01}Bi_{0.06}Te$ sample (~200 H_v) reveals its high mechanical stability. High thermoelectric figure of merit and enhanced mechanical stability motivates us to measure the power conversion efficiency of single-leg TE devices based on In and Bi co-doped GeTe. We obtained extremely high estimated thermoelectric conversion efficiency (η) of ~12.3% in single-leg $Ge_{0.93}In_{0.01}Bi_{0.06}Te$ TE generator for the temperature difference of 445 K. The obtained power conversion efficiency is the highest among the single-leg-based thermoelement (non-segmented) in the ΔT range of 400–600 K.

[1]New Chemistry Unit, Jawaharlal Nehru Centre for Advanced Scientific Research (JNCASR), Jakkur P.O., Bangalore 560064, India

[2]Theoretical Sciences Unit, Jawaharlal Nehru Centre for Advanced Scientific Research (JNCASR), Jakkur P.O., Bangalore 560064, India

[3]Technical Physics Division, Bhabha Atomic Research Centre (BARC), Mumbai 400085, India

[4]School of Advanced Materials and International Centre of Materials Science, Jawaharlal Nehru Centre for Advanced Scientific Research (JNCASR), Jakkur P.O., Bangalore 560064, India

[5]Present address: Department of Physics and Nanotechnology, SRM Institute of Science and Technology, Kattankulathur, Chennai 60203, India

[6]These authors contributed equally

[7]Lead Contact

*Correspondence: kanishka@jncasr.ac.in

https://doi.org/10.1016/j.joule.2019.08.017

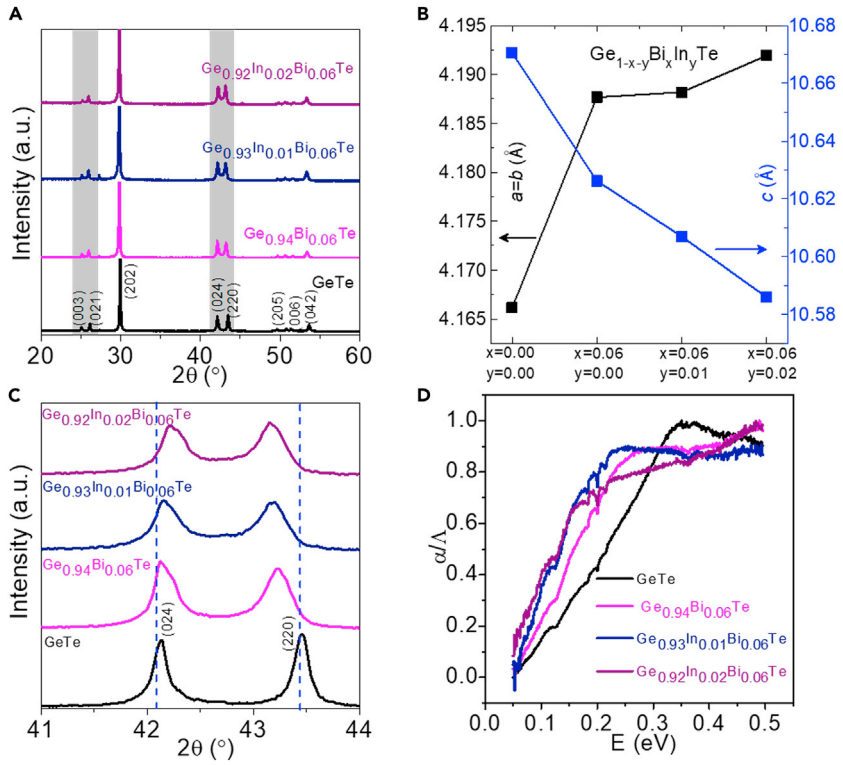

Figure 1. Structural Characterization and Optical Band Gap

(A) Powder XRD patterns of $Ge_{1-x-y}Bi_xIn_yTe$ (x = 0.06; y = 0, 0.01, and 0.02) samples.

(B) The lattice constants of $Ge_{1-x-y}Bi_xIn_yTe$ as a function of the composition.

(C) Zoomed-in version of PXRD pattern of Figure 1A in the angles (2Θ) between 41° and 44°, indicating the evolution of (024) and (220) peaks with co-doping of In and Bi.

(D) Electronic absorption spectra of $Ge_{1-x-y}Bi_xIn_yTe$ samples.

RESULTS AND DISCUSSION

Samples of $Ge_{1-x-y}Bi_xIn_yTe$ (x = 0–0.06, y = 0–0.02) were synthesized by vacuum-sealed tube melting reaction and their structures are initially analyzed by powder X-ray diffraction (PXRD). Figure 1A shows the PXRD patterns of $Ge_{1-x-y}Bi_xIn_yTe$, and all the obtained patterns could be matched with the rhombohedral structure (α-GeTe, space group *R3m*). Low-intensity peaks corresponding to excess Ge were identified in all the patterns which often arise due to the presence of thermodynamically driven cation (Ge) vacancies in GeTe, agreeing with the previous reports.[25–27] The high-intensity peak at 2θ = 29.88° in pristine GeTe gradually shifts toward lower angle with increasing Bi and In concentration due to the replacement of smaller Ge (1.25Å) atoms by larger Bi (1.43Å) and In (1.56Å) (Figure S1). Figure 1B shows the calculated lattice constants of $Ge_{1-x-y}Bi_xIn_yTe$. The lattice parameters of pristine GeTe are *a* = *b* = 4.1664(2) Å, *c* = 10. 6707(4) Å, whereas $Ge_{0.94}Bi_{0.06}Te$ exhibits the lattice constants of *a* = *b* = 4.1876 (8) Å, *c* = 10.6262 (5) Å indicating that addition of Bi increases *a* and *b* axes with the contraction along the *c* axis, which conforms with the previous reports of Bi and Bi-Sb co-doped GeTe.[27,38] Moreover, the substitution of In in $Ge_{0.94}Bi_{0.06}Te$ further increases *a* and *b* axes and reduces *c* axis, as seen in Figure 1B. Figure 1C illustrates the zoomed-in version of the double peaks present between the 2θ angles of 41° and 44°, which further confirms the rhombohedral structure (α-GeTe) at room temperature. The double peaks from (024) and (220) planes get closer upon Bi and In co-doping in GeTe. This is a clear indication

that co-doping of Bi and In in GeTe drives the system toward cubic (space group *Fm-3m*) structure by relaxing the structure along [111] direction.

Figure 1D presents the electronic absorption spectra of $Ge_{1-x-y}Bi_xIn_yTe$ samples as a function of energy (*E*). Pristine GeTe has a band gap of ~0.21 eV, which is consistent with the previous reports.[26,27,38] The addition of Bi notably reduces the band gap of GeTe from 0.21 to 0.12 eV and In doping further decreases the band gap to 0.08 eV. Because of the higher electronegativity (χ_{Te} = 2.10 in Pauling scale), Te orbitals predominantly constitutes the valence band of GeTe, whereas Ge orbitals predominately contribute to the conduction band because of its lower electronegativity (χ_{Ge} = 2.01). The reduction in band gap is mainly due to the formation of impurity states of Bi and In just below the conduction band because of their donor dopant nature and the slightly higher electronegativity of Bi (~2.02) than Ge. Electronic structure of Bi- and In-doped GeTe calculated from DFT further confirms the formation of Bi and In-induced states below the conduction band of GeTe, which we have discussed later.

Figure 2 depicts the TEM micrographs of $Ge_{0.93}Bi_{0.06}In_{0.01}Te$ samples, investigated using an aberration-corrected TEM. Figure 2A shows the low magnification TEM micrograph of $Ge_{0.93}Bi_{0.06}In_{0.01}Te$ exhibiting the ordered domain variants of bright and dark contrast in the <110> direction. Generally, the consecutive contrast difference with a regular interval arises due to the breakdown of Friedel symmetry in noncentrosymetric crystals.[25–27] Doping of Bi alone in GeTe does not introduce any such domain variants,[38] however, the addition of 1 mol % of In in $Ge_{0.94}Bi_{0.06}Te$ results in the formation of ordered domain variants. A clear selected area electron diffraction (SAED) pattern is shown in inset Figure 2A, which confirms the highly crystalline nature. High-resolution TEM micrograph of a region from Figure 2A is shown in Figure 2B, which depicts the lattice spacing of ~0.3 nm that corresponds to the (202) plane in rhombohedral GeTe. The presence of reflection twins along <110> direction with distinguishable ordered domain variants in the form of herringbone structure is observed in $Ge_{0.93}Bi_{0.06}In_{0.01}Te$ (see Figure 2C). The corresponding SAED pattern (Figure 2D) along the zone axis of <110> exhibits spot splitting, which further confirms the existence of twins. These domain variants, along with solid solution point defects, would be expected to scatter large amounts of mid-wavelength phonons and thereby reduce the κ_{lat} (discussed later).

The temperature dependence of electrical conductivity, σ, of $Ge_{1-x-y}Bi_xIn_yTe$ (x = 0–0.06, y = 0–0.02) is presented in Figure 3A. The σ of all the samples decreases with increasing temperature, indicating the degenerate semiconductor behavior. At 300 K, pristine GeTe shows the σ value of 8,067 S/cm, which reduces to 2,158 S/cm at 708 K. Above 675 K, σ starts increasing due to the second-order structural transition (*R3m* → *Fm-3m*). Co-doping of In and Bi in GeTe drastically reduces the σ values throughout the measured temperature range due to the suppression of Ge vacancies and the donor dopant nature of In^{3+} and Bi^{3+} at Ge^{2+} sites, which decreases the hole density by offering excess electrons. In particular, the room temperature σ value of ~8,067 S/cm in GeTe decreases to ~970 S/cm in $Ge_{0.92}Bi_{0.06}In_{0.02}Te$. The substitution of Bi and In in GeTe gradually decreases the structural transition temperature from 675 K in GeTe to 525 K in $Ge_{0.92}Bi_{0.06}In_{0.02}Te$, which is evident from the change in slope near the phase transition temperature in σ versus T data (Figures 3A and S2).

To examine the reduction in σ values in the Bi and In co-doped GeTe, room temperature Hall measurements were performed for all the samples of $Ge_{1-x-y}Bi_xIn_yTe$.

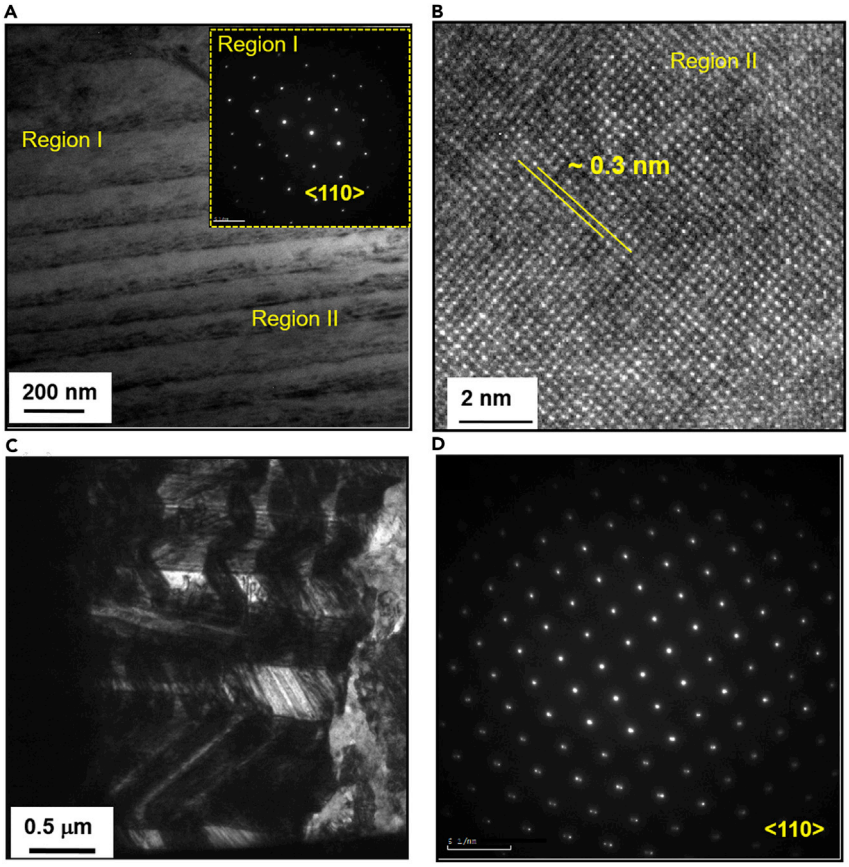

Figure 2. Transmission Electron Micrographs

(A) Low magnification TEM micrograph of $Ge_{0.93}Bi_{0.06}In_{0.01}Te$ with ordered domain variants of dark and bight contrast difference. Inset of (A) shows the corresponding SAED, indicating high quality single crystalline nature.

(B) HRTEM micrograph of $Ge_{0.93}Bi_{0.06}In_{0.01}Te$ depicts an interplanar spacing of 0.3 nm corresponding to (202) plane of α-GeTe (*R3m*).

(C) The existence of reflection twins with herringbone structure along <110> zone axis.

(D) SAED pattern with spot splitting confirms the presence of twins.

p-type carrier density (*n*) of undoped GeTe is 5.87 × 10^{20} cm^{-3}, which reduces to 2.1 × 10^{20} cm^{-3}, 2.17 × 10^{20} cm^{-3}, 3.13 × 10^{20} cm^{-3}, and 1.59 × 10^{20} cm^{-3} in $Ge_{0.94}Bi_{0.06}Te$, $Ge_{0.94}In_{0.06}Te$, $Ge_{0.93}Bi_{0.06}In_{0.01}Te$, and $Ge_{0.92}Bi_{0.06}In_{0.02}Te$, respectively (Table S1). The suppression of *p*-type carrier density is due to the aliovalent dopants of In^{3+} and Bi^{3+} at Ge^{2+} site in GeTe as they provide excess electron to the system. Further, the estimated carrier mobility (μ) of different $Ge_{1-x-y}BixIn_yTe$ samples (Table S1) shows that while Bi-doped GeTe samples retain the high mobility, In-doped and Bi, In co-doped samples have significantly lower mobility than that of the pristine GeTe. In doping in GeTe is known to create resonance level near the Fermi energy.[33] The observed reduced mobility of the present In-doped samples corroborates with such resonant scattering scenario of charge carriers.[33]

Temperature dependence of Seebeck coefficient, *S*, of $Ge_{1-x-y}Bi_xIn_yTe$ is presented in Figure 3B. The *S* values of all the measured samples are of a positive sign, which implies that holes are the majority carries in $Ge_{1-x-y}Bi_xIn_yTe$, supporting the Hall coefficient data. The *S* values of all the samples increase with a rise in temperature in the measured temperature range. Typically, the *S* value of pristine GeTe is ~34 μV/K at

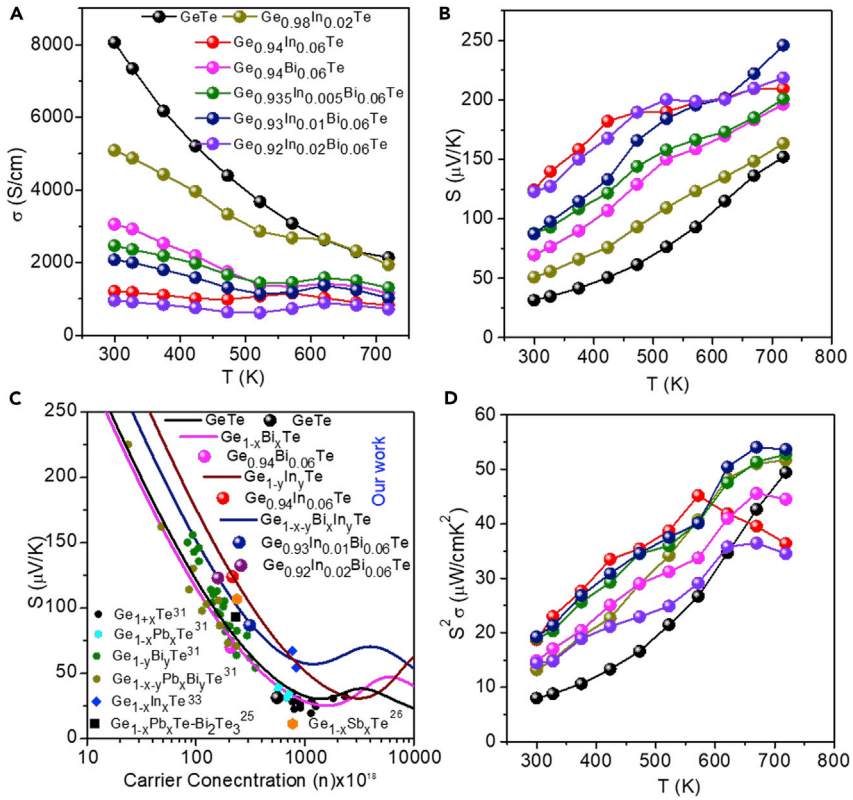

Figure 3. Electrical Transport and Thermopower

(A and B) Temperature-dependent (A) electrical conductivity (σ) and (B) Seebeck coefficient (S) of $Ge_{1-x-y}Bi_xIn_yTe$ samples.

(C) Calculated Pisarenko plots considering two valance band model (solid lines) and the experimental *S* versus *n* data points of the In and Bi co-doped GeTe compared with previously reported *S* versus *n* data of different GeTe-based samples.[25,31,33,26]

(D) Temperature-dependent power factor ($S^2\sigma$) of $Ge_{1-x-y}Bi_xIn_yTe$ samples.

300 K, which substantially increases to ~153 μV/K at 720 K. The inverse relation of *S* and *n* leads to increase in *S* values as doping of In and Bi in GeTe leads to significant suppression of *p*-type carrier density. In particular, doping of 6 mol % Bi in GeTe increases *S* value from 32 μV/K to ~70 μV/K at 300 K, whereas 6 mol % of In doping shows drastic enhancement in *S* value to 125 μV/K, which is about 290% improvement in *S* value than that of pristine GeTe. This large enhancement in *S* upon In doping is associated with distortion of the DOS of GeTe due to the formation of resonant states close to Fermi level, E_F, and is discussed in a later section.[33] Moreover, it is clearly seen that the increase in In concentration in $Ge_{0.94}Bi_{0.06}Te$ substantially enhances the S values. Typically, the S value of $Ge_{0.94}Bi_{0.06}Te$ is ~70 μV/K at 300 K, which increases to ~86 μV/K, ~89 μV/K, and ~122 μV/K in $Ge_{0.935}Bi_{0.06}In_{0.005}Te$, $Ge_{0.93}Bi_{0.06}In_{0.01}Te$, and $Ge_{0.92}Bi_{0.06}In_{0.02}Te$, respectively. The obtained maximum *S* value is ~246 μV/K at 720 K in the $Ge_{0.93}Bi_{0.06}In_{0.01}Te$ sample.

To understand the carrier concentration-dependent Seebeck coefficient of individual and Bi and In co-doped GeTe, the experimental room temperature *S* values were compared with calculated Pisarenko plot (*S* versus *n*) considering two valance band model[15,31,40] (Figure 3C; Table S2). In the two valance band model, the total Seebeck coefficient has the contribution from both the heavy hole valance band (S_{hh}) and light hole valance band (S_{lh}). The heavy hole valance band is considered

as non-parabolic with a non-parabolicity factor k_BT/E_g (E_g is the band gap), while the light hole valance band far below the Fermi level is considered as parabolic. The values of acoustic deformation potentials are taken from the literature.[40] The calculated Pisarenko plot for pristine GeTe matches well with the previously reported data as well as with the present data (Figure 3C). At room temperature, the contribution of S_{lh} to the total Seebeck coefficient is, however, negligible in pristine GeTe owing to the large energy gap between the heavy and light hole valance band (Δ = 0.23 eV).[25,41] From the Pisarenko analysis, we find that although Bi-doped GeTe has higher room temperature Seebeck coefficient, the enhancement is entirely due to the decrease in carrier concentration caused by Bi^{3+} doping in place of Ge^{2+}. The large enhancement in the Seebeck coefficient in the In-doped GeTe samples, on the other hand, can only be accounted by the drastic increase in the effective mass of the heavy hole valance band ($m_{hh} = 2.4\ m_0$). Such drastic increase in effective mass of the heavy hole valance band upon In doping indicates distortion in the electronic DOS by the formation of resonance level close to the Fermi energy.[33] While the band gap, E_g, decrease in both cases of the individual In and Bi doping, Δ remains unaltered. In case of In and Bi co-doping, the Pisarenko analysis of the room temperature Seebeck coefficient exhibits that along with an increase in the effective mass of the heavy hole valance band ($m_{hh} = 1.9\ m_0$), the gap between two valence bands (Δ) also decreases to 0.16 eV. The decrease in Δ indicates the presence of valance band convergence effect between the heavy and light hole valance band at room temperature in Bi- and In-doped GeTe.

We used DFT calculations to determine the electronic structures of doped and undoped GeTe compositions for further understanding the experimentally observed thermoelectric transport behaviors. Electronic structure of valence and conduction bands of rocksalt GeTe is similar to that of SnTe and PbTe, with 4 extrema at L point and 12 extrema along Σ line in the Brillion zone (BZ).[44] GeTe undergoes a cubic to rhombohedral phase transition at ~700 K, breaking the inversion symmetry in the low-temperature rhombohedral phase. Since the rhombohedral phase of GeTe is nearly cubic with minor lattice distortions and the cubic phase is relevant to the thermoelectric performance at high-temperatures, we analyze the electronic structure of doped and undoped GeTe in the cubic phase, similar to the earlier works.[25,27] Because of the Brillouin zone folding associated with the ($\sqrt{2} \times \sqrt{2} \times 2$) supercell used in the calculations here, the principal valence band maximum (VBM) occurring normally at L point of the cubic cell, occurs at Γ point, and the conduction band minimum (CBM) also folds back to Γ point. The heavy hole valence band maximum occurring along Σ line of the cubic BZ, appears at Z + δ along Z→R direction in the Brillouin zone of ($\sqrt{2} \times \sqrt{2} \times 2$) tetragonal supercell.[27] Electronic structure of $Ge_{16}Te_{16}$ (Figure 4A) exhibits a band gap of ~0.19 eV at Γ point, which is in good agreement with the previous electronic structure calculations.[25,27] The energy difference between the light and heavy hole valence bands, $\Delta \sim 0.20$ eV. Although in the DFT calculated electronic structure, the Fermi level resides in the middle of the band gap between VBM and CBM in pristine GeTe, a large amount of Ge vacancies in the experimentally synthesized GeTe samples cause the Fermi level to move deep inside the valance band resulting its *p*-type thermoelectric transport behavior.[33,41]

In pristine GeTe, the Ge-*p* orbitals form the CBM, while the Te-*p* orbitals dominate the VBM. In 6.25 mol % Bi-substituted GeTe, a new impurity band associated with the Bi-*p* orbital forms in the energy gap between VBM and CBM (Figure 4B). The more electronegative character of Bi compared to Ge and the donor dopant nature of Bi results in the shift of CBM downward in energy. This is reflected in the lower band gap in Bi-doped GeTe compositions. The energy difference between the light

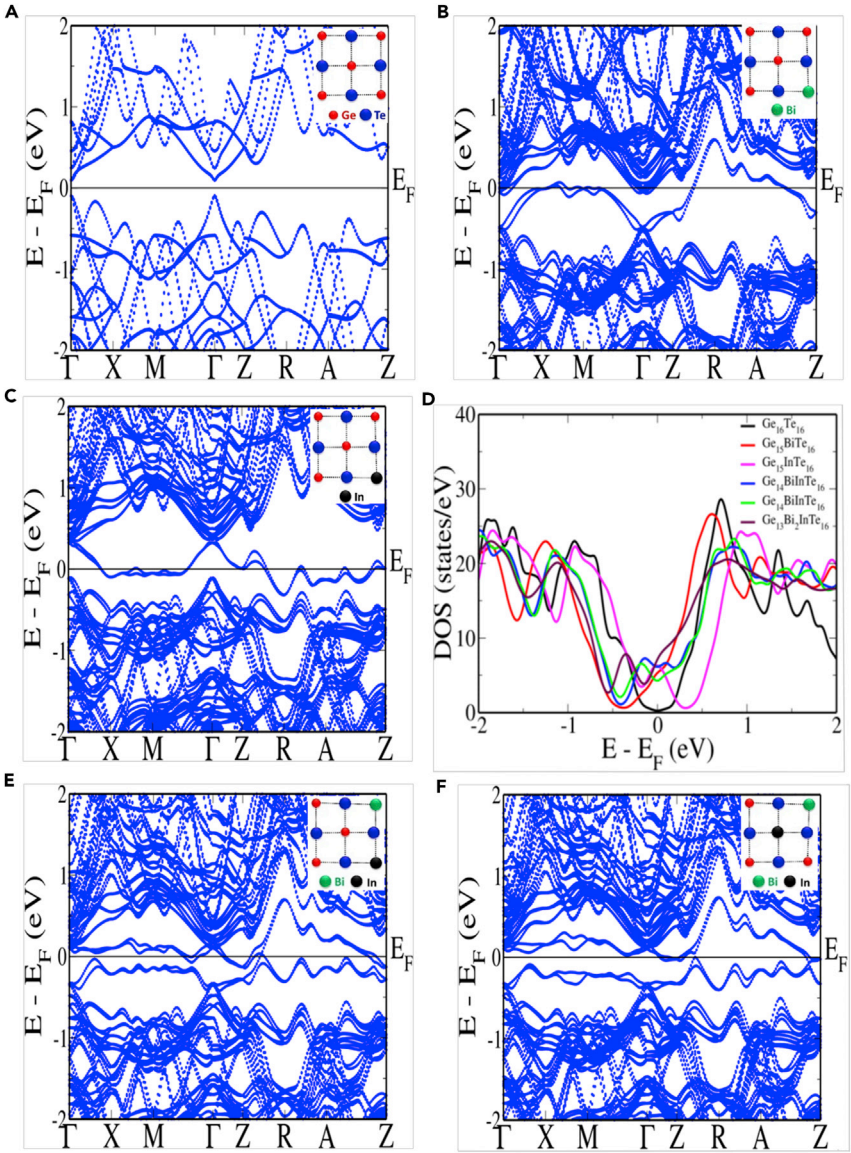

Figure 4. Electronic Structure

(A–C) Electronic structures of (A) $Ge_{16}Te_{16}$, (B) $Ge_{15}BiTe_{16}$, and (C) $Ge_{15}InTe_{16}$.

(D) Density of electronic states of pure GeTe and Bi-, In-, and co-doped (Bi and In) GeTe samples. Solid blue line and green lines represent the cases where Bi and In atoms are far and close to each other, respectively.

(E and F) Electronic structures of (E) $Ge_{14}BiInTe_{16}$ (Bi and In atoms far from each other) (F) $Ge_{14}BiInTe_{16}$ (Bi and In atoms close to each other).

hole and heavy hole valence band, however, remains essentially unchanged ~0.201 eV in Bi-doped GeTe, which further corroborates to the Pisarenko plot analysis of the room temperature Seebeck coefficient. Indium (In) substitution in GeTe also introduces impurity band in the energy gap between VBM and CBM similar to the Bi doping; however, the salient feature of the electronic structure is very different. In the case of In doping, the impurity band is much weakly dispersed near the Fermi energy, leading to the formation of resonance level close to the Fermi level, as seen in Figures 4C and 4D. The formation of resonance level with the weakly

dispersed band near the Fermi energy results in increased effective mass which is reflected in the increased room temperature Seebeck coefficient and further supports the increased effective mass of the heavy hole valance band obtained from the Pisarenko analysis. As reported in the earlier investigations,[33] we also found that the deep defect states of pristine GeTe move upward toward Fermi energy due to the hybridization of In-*p* orbital with the host.

DFT calculation of electronic structures for the individual doping of In and Bi in GeTe indicates their distinct roles: while Bi doping results in the formation of impurity bands close to the CBM, In doping causes the formation of resonance level close to the Fermi energy. Therefore, to understand the modulation of electronic structure in case of Bi and In co-doped GeTe, we considered various configurations of their co-doping. Here, we have shown two particular interesting configurations: (1) one with Bi and In atoms close to each other (Figure 4F) and (2) another with Bi and In atoms far from each other (Figure 4E). We find that two almost parallel bands form in the gap between VBM and CBM and reside on the two sides of E_F. Interestingly, these bands mix with each other between Z and R points of the BZ, and their interaction gives rise to multiple minima and maxima in both valence and conduction bands at closely spaced energies. Although the resonance level forms in this co-doping case also, as can be seen from Figure 4D, the resonance level moves away from the Fermi energy and deeper toward the valance band. Consequently, the distortion in the electronic DOS decreases, and this is further reflected in the Pisarenko analysis of the room temperature Seebeck coefficient, which indicates lower effective mass of the heavy hole valance band in case of In and Bi co-doped GeTe compared to individual In-doped GeTe. With increasing Bi concentration in this Bi and In co-doped GeTe, the impurity bands hybridize more strongly with the host (Figure S3), which further pushes the resonance level deeper inside the valance band. Surprisingly, we observed that co-doping of Bi and In results in decreasing energy difference between the heavy and light hole valance band to 0.10 eV compared to 0.20 eV in case of pristine GeTe. We have observed similar valance band convergence effect in the Pisarenko analysis of the room temperature Seebeck coefficient in In and Bi co-doped GeTe. As can be seen from Figure 4, In impurity states hybridize much more effectively with the host valance states in case of Bi and In co-doped GeTe compared to individual In doping, which results in the observed decrease in energy difference between heavy and light hole valance band.[44] The increased interaction of In with the host valance states is also probed using Kelvin probe force microscopy (KPFM). With increasing In concentration in the In and Bi co-doped system, the increased interaction between the impurity and host decreases the p-type carrier concentration which is evident from the decreased work function as obtained from KPFM (Table S3).

Figure 3D presents the power factor, $S^2\sigma$, of $Ge_{1-x-y}Bi_xIn_yTe$ (x = 0–0.06, y = 0–0.02) as a function of temperature, which exhibits that power factor increases with rise in temperature. Typically, undoped GeTe has the $S^2\sigma$ value of ~8.1 $\mu Wcm^{-1}K^{-2}$ at 300 K, and it reaches to the maximum value of ~49.2 $\mu Wcm^{-1}K^{-2}$ at 720 K. Additionally, the 6 mol % Bi-doped GeTe sample shows the $S^2\sigma$ values of ~14.8 and ~45.4 $\mu Wcm^{-1}K^{-2}$ at 300 and 675 K, respectively, whereas $S^2\sigma$ values of $Ge_{0.98}In_{0.02}Te$ are ~13.2 and ~51.6 $\mu Wcm^{-1}K^{-2}$ at 300 and 675 K, respectively. Further, the addition of In in $Ge_{0.94}Bi_{0.06}Te$ substantially increases the values of $S^2\sigma$ in the measured temperature range of 300–725 K. In particular, the $S^2\sigma$ value of $Ge_{0.93}Bi_{0.06}In_{0.01}Te$ is ~19.3 $\mu Wcm^{-1}K^{-2}$ at 300 K, which increases with temperature and reaches to the value of ~53.7 $\mu Wcm^{-1}K^{-2}$ at 720 K. This large enhancement in $S^2\sigma$ value is due to the formation of In-induced resonant states and Bi-driven

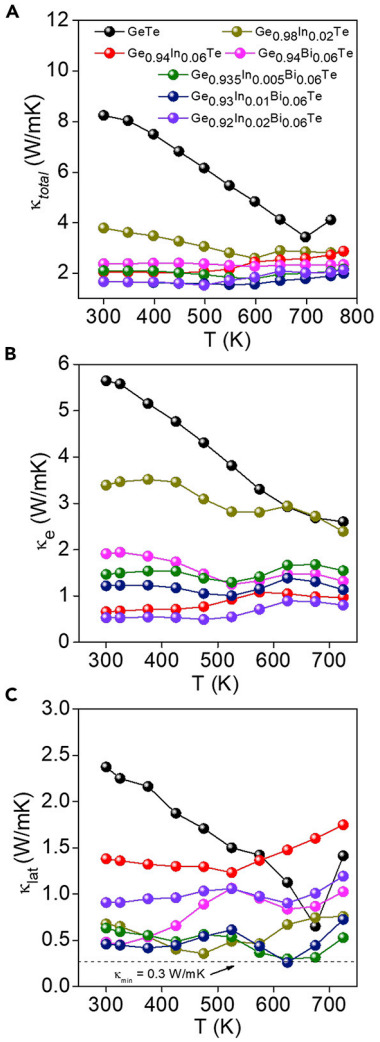

Figure 5. Thermal Conductivity

(A–C) Temperature-dependent total thermal conductivity (κ_{total}) (A), electronic thermal conductivity (κ_e) (B), and lattice thermal conductivity (κ_{lat}) (C) of $Ge_{1-x-y}Bi_xIn_yTe$ samples.

suppression in *p*-type carrier concentration. Figure S4 illustrates the power factor for different GeTe-based materials,[6,20,25–34,38] which shows that $Ge_{0.93}Bi_{0.06}In_{0.01}Te$ exhibits remarkably high $S^2\sigma$ value of 54.3 $\mu Wcm^{-1}K^{-2}$ compared to the previously reported GeTe-based materials.

Temperature-dependent total thermal conductivity, κ_{total}, of $Ge_{1-x-y}Bi_xIn_yTe$ (x = 0–0.06, y = 0–0.02) is shown in Figure 5A, which exhibits that κ_{total} substantially reduces with increase in temperature, as often seen in typical degenerate semiconducting solids. κ_{total} of pristine GeTe is ~8.3 W/mK at 300 K, which gradually reduces to the minimum value of ~3.4 W/mK at 673 K. Above 675 K, κ_{total} starts increasing due to Ge translation along <111> direction-induced second-order structural transition (*R3m* → *Fm-3m*), which is also observed in σ versus *T* data in Figures 3A and S2. The addition of individual dopants of In and Bi in GeTe rapidly reduces κ_{total} to ~3.8 and ~2.28 W/mK at 300 K for the compositions of $Ge_{0.98}In_{0.02}Te$ and $Ge_{0.94}Bi_{0.06}Te$, respectively. In addition, co-doping of In and

Bi in GeTe further decreases the κ_{total} to ~1.68 W/mK at 300 K which moderately comes down with temperature and reaches the minimum value of ~1.55 W/mK at 500 K in the composition of $Ge_{0.92}In_{0.02}Bi_{0.06}Te$.

Figure 5B presents the electronic contribution to thermal conductivity, κ_e, of $Ge_{1-x-y}Bi_xIn_yTe$ (x = 0–0.06, y = 0–0.02) as a function of temperature. κ_e is calculated form Wiedemann-Franz law, $\kappa_e = \sigma \cdot L_0 \cdot T$, where L_0 is the Lorenz number. The temperature-dependent L_0 is obtained by estimating the reduced chemical potential from temperature-dependent Seebeck coefficient considering a single parabolic band model[25–27] (Figure S5C). The κ_e of GeTe is ~5.65 W/mK at 300 K, which shows that *p*-type carriers have a dominant contribution to κ_{total}. Co-doping of In and Bi in place of Ge in GeTe largely suppresses the Ge vacancies and reduces the hole density, thereby significantly decreasing the κ_e values to ~0.55 W/mK at 300 K for the composition of $Ge_{0.92}In_{0.02}Bi_{0.06}Te$.

The κ_{lat} of $Ge_{1-x-y}Bi_xIn_yTe$ (x = 0–0.06, y = 0–0.02) samples are estimated by subtracting the κ_e from κ_{total} and temperature-dependent κ_{lat} is shown in Figure 5C. The κ_{lat} of GeTe is ~2.4 W/mK at 300 K, which subsequently decreases with increasing temperature and reaches the minimum value of ~0.67 W/mK near the phase transition temperature (~675 K), and above 675 K, the κ_{lat} of GeTe starts increasing. This fact is mainly ascribed to the ferroelectric instability near phase transition temperature as it induces soft optical phonon modes which strongly scatter the heat-carrying acoustic phonons.[26] Addition of 6 mol % of Bi in GeTe decreases the κ_{lat} value to ~0.67 W/mK at 300 K, whereas 6 mol % of In doping results in κ_{lat} ~ 1.38 W/mK at 300 K. This indicates the effective role of Bi doping in reducing κ_{lat} of GeTe. Interestingly, $Ge_{0.93}In_{0.01}Bi_{0.06}Te$ has κ_{lat} ~ 0.27 W/mK at 625 K, which is very close to the theoretical κ_{min} (~0.3 W/mK) of GeTe.[27,28] This large reduction in κ_{lat} could be attributed to the strong phonon scattering by the collection of (1) solid solution point defects, (2) domain variants, and (3) twin boundaries with herringbone structures, which were observed in the TEM micrographs (Figures 2A and 2C).

Figure 6A illustrates the dimensionless figure of merit, *zT*, of $Ge_{1-x-y}Bi_xIn_yTe$ (x = 0–0.06, y = 0–0.02) as a function of temperature. Pristine GeTe exhibits maximum *zT* of 0.9 at 675 K.[22] Further, the maximum *zT* of 1.31 and 1.38 at 725 K are achieved in the controlled compositions $Ge_{0.98}In_{0.02}Te$ and $Ge_{0.94}Bi_{0.06}Te$, respectively, consistent with the previous reports.[12a,14b] Interestingly, In and Bi co-doping in GeTe remarkably increases the *zT*. Specifically, the *zT* of $Ge_{0.93}In_{0.01}Bi_{0.06}Te$ reaches the maximum value of 2.1 at 723 K, which is ~233% higher than that of the pristine GeTe. High *zT* samples were re-measured and taken for cyclic measurement (heating and cooling cycle), which exhibits good heating-cooling reversibility and reproducibility (see Figure S6). We would like to point out that, if we calculate *zT* based on the thermal conductivity obtained using Dulong-Petit heat capacity (C_p, Figure S5B) value, the maximum *zT* in $Ge_{0.93}In_{0.01}Bi_{0.06}Te$ would be ~2.5 at 723 K (Figure S7). Although in few recent reports *zT* has been calculated based on the Dulong-Petit C_p value,[31–34,40,41] we believe it is better to use measured C_p for the estimation of thermal conductivity and *zT*, which will reduce the error in zT estimation. Thus, we have used maximum *zT* of 2.1 for further calculation of zT_{avg} and ZT_{eng} (see later). The composition of $Ge_{0.93}In_{0.01}Bi_{0.06}Te$ possess the zT_{avg} of ~1.3, which is significantly high as compared to the recently reported GeTe-based materials, such as $Ge_{0.94}Bi_{0.06}Te$, $Ge_{0.9}Sb_{0.1}Te$, 3% Bi_2Te_3 added $Ge_{0.87}Pb_{0.13}Te$, TAGS80, TAGS85, $Ge_{0.98}In_{0.02}Te$, $Ge_{0.86}Sb_{0.04}Mn_{0.1}Te$ and so on.[20,25–29,33,37,38] Mention must be made that the present In and Bi co-

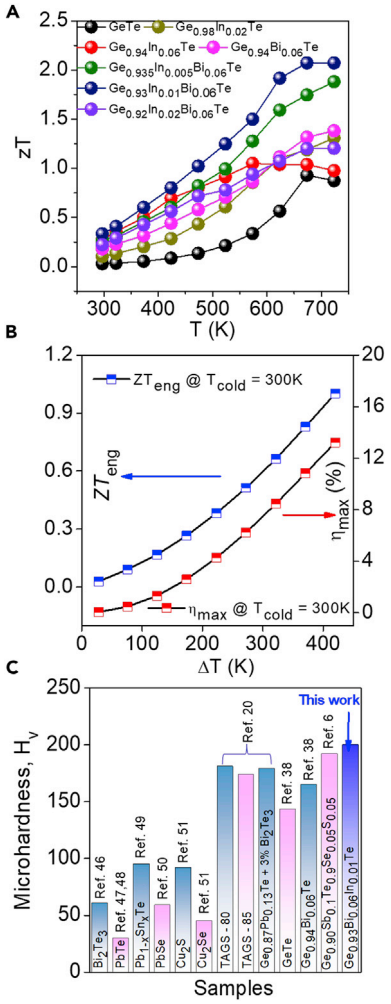

Figure 6. Thermoelectric Figure of Merit

(A) Temperature-dependent thermoelectric figure of merit (zT) of $Ge_{1-x-y}Bi_xIn_yTe$ system.

(B) Calculated engineering figure of merit (ZT_{eng}) and efficiency (η) of $Ge_{1-x-y}Bi_xIn_yTe$ system as a function of temperature difference, respectively.

(C) Histogram representing Vickers microhardness value of $Ge_{0.93}In_{0.01}Bi_{0.06}Te$ along with other state-of-the-art metal chalcogenides.

doped GeTe show significantly high zT compared to the previously reported In and Bi co-doped GeTe ($zT \sim 0.85$) by Srinivasan et al.[39]

As the calculation of TE conversion efficiency (η) based on the materials figure of merit, zT, is not very reliable due to the major assumption of temperature-independence of S, σ, and κ_{total}, Kim et al.[45] have recently introduced the engineering figure of merit, ZT_{eng}, and the maximum efficiency, η (ZT_{eng}), based on the cumulative temperature-dependent properties which has been used here to reliably calculate the η with large temperature difference. Here, we have calculated the ZT_{eng} and η (ZT_{eng}) of $Ge_{0.93}In_{0.01}Bi_{0.06}Te$ as a function of temperature difference of the cold and hot sides (see Figure 6B), in which T_C is assumed as 300 K in the calculation. The maximum ZT_{eng} of $Ge_{0.93}In_{0.01}Bi_{0.06}Te$ is calculated to be ~1, whereas the highest η (ZT_{eng}) is determined as ~13.3% for the temperature difference ΔT = 420 K (see Figures 6B and S8).

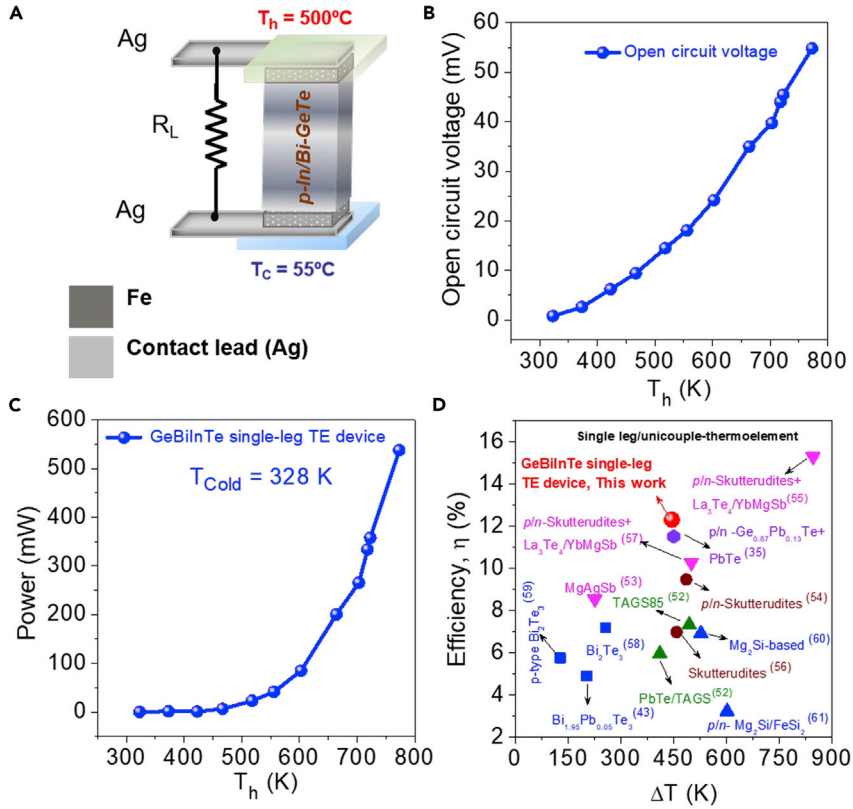

Figure 7. Power Conversion Efficiency of Single-Leg TE Device

(A) The schematic diagram of single-leg *p*-type $Ge_{0.93}Bi_{0.06}In_{0.01}Te$-based single-leg TE device.
(B and C) Open-circuit voltage (V_{OC}) (B) and output power (P_w) (C) as a function of T_h.
(D) Comparison of the efficiency of the present single-leg-based In and Bi co-doped GeTe thermoelement with other state-of-the-art single-leg- and unicouple-based thermoelectric device (non-segmented based).[35,43,52–61]

Further, in order to check the mechanical stability of the high-performance Bi and In co-doped GeTe, Vickers microhardness of $Ge_{0.93}Bi_{0.06}In_{0.01}Te$ is measured, and it is found to be ~200 H_v (kgf/mm^2), which is comparatively higher than that of the undoped GeTe (H_v ~ 143). Reduced Ge vacancies and enhanced atomic mixing in In and Bi co-doped GeTe inhibits the propagation of nano- and micro-cracks and thus increases the mechanical stability of the material compared to pristine GeTe. A comparison of H_v values of different state-of-the-art metal chalcogenides and $Ge_{0.93}Bi_{0.06}In_{0.01}Te$ are presented in Figure 6C.[6,20,26,38,46–51]

Motivated by the calculated high η (ZT_{eng}) and enhanced microhardness of the Bi and In co-doped GeTe samples, we have successfully fabricated single-leg-based TE devices with the high zT *p*-type $Ge_{0.93}In_{0.01}Bi_{0.06}Te$ sample. A complete schematic diagram of the $Ge_{0.93}In_{0.01}Bi_{0.06}Te$-based single-leg thermoelement with diffusion barrier (Fe) and contact layers (Ag) connected with load resistance is depicted in Figures 7A and S9. The open-circuit voltage of the device as a function of hot-end temperature (T_h) is shown in Figures 7B and S10B. We find that the experimental open-circuit voltage (V_{OC}) of the device enhances with increasing T_h due to increasing temperature difference (ΔT) and enhanced Seebeck coefficient (S) of the TE material at higher temperatures, and the V_{OC} reaches the maximum value of 55 mV at 773 K. The plot of electrical power output generated (i.e., $P_W = I_L \times V_L$)

as a function of T_h is shown in Figure 7C, which increases with increasing hot-end temperature and the maximum power output of ~538 mW is obtained for the maximum operating temperature of 773K. The estimated TE conversion efficiency, η, of single-leg $Ge_{0.93}In_{0.01}Bi_{0.06}Te$ TE generator is estimated by taking the ratio of experimental electrical output power (P_W) to estimated input heat flowing (Q_H) across the thermoelement and the maximum η of ~12.3% was obtained for the temperature difference of ΔT = 445 K (see Figures 7D and S11). We have compared this remarkable high efficiency of single-leg-based $Ge_{0.93}In_{0.01}Bi_{0.06}Te$ TE device with other reported single-leg or unicouple-based devices (non-segmented),[35,42,43,52–61] which shows that the present single-leg $Ge_{0.93}In_{0.01}Bi_{0.06}Te$ TE device exhibits the highest η in the ΔT range of 450–600 K. Mention must be made that at ΔT = 445 K, the measured values of output power density (P_d) and estimated efficiency (η) are ~1.1 W/cm^2 and 12.3%, respectively, which are comparatively lower than the respective simulated values (P_{deng} = 1.7 W/cm^2 and η (ZT_{eng}) = 13.3% for ΔT = 420 K, Figures 6B and S8) because of the added electrical resistance at different material interfaces in the fabricated device.[62–65]

In conclusion, we have demonstrated a very high zT of 2.1 at 723 K along with high zT_{avg} of ~1.3 in the temperature range of 300–723 K in In and Bi co-doped GeTe. Aliovalent Bi doping in GeTe effectively optimized the p-type carrier density and reduced the lattice thermal conductivity by the formation of extensive point defects and domain variants. On the other hand, In doping in GeTe leads to the formation of resonant states close to the Fermi level which consequently distorts DOS and accounts for the huge enhancement in Seebeck coefficient. The co-doping of In and Bi in GeTe leads to distinct but complementary contributions to modulate the electronic structure and thermal transport of GeTe and hence results in high thermoelectric performance. Moreover, the measured Vickers microhardness of $Ge_{0.93}In_{0.01}Bi_{0.06}Te$ of 200 H_v (kgf/mm^2) reflects the high mechanical stability of the material. The fabricated single-leg TE devices based on In and Bi co-doped GeTe shows high output power of ~538 mW and extremely high estimated thermoelectric efficiency of 12.3% for the temperature difference of 445 K.

EXPERIMENTAL PROCEDURES

Full details of experimental procedures can be found in the Supplemental Information.

SUPPLEMENTAL INFORMATION

Supplemental Information can be found online at https://doi.org/10.1016/j.joule.2019.08.017.

ACKNOWLEDGMENTS

This work was partially supported by DST (DST/TMD/MES/2k17/24) and Sheikh Saqr Laboratory. M.S. thanks UGC for her fellowship. U.V.W. acknowledges funding from IKST, Sheikh Saqr fellowship, and J C Bose National Fellowship of the DST.

AUTHOR CONTRIBUTIONS

Conceptualization, K.B.; Experiments, S.P., M.S., T.G., K.B., A.K.B., S.B., and A.S.; DFT calculations, U.S.S. and U.V.W.; Analysis and Discussion, K.B., S.P., M.S., T.G., U.V.W., and S. B.; Writing and Revision, K.B., S.P., M.S., T.G., U.S.S., U.V.W., A.K.B., S.B., and A.S.

DECLERATION OF INTERESTS

The authors declare no competing interests.

Received: April 29, 2019
Revised: June 20, 2019
Accepted: August 21, 2019
Published: September 20, 2019

REFERENCES

1. Tan, G., Zhao, L.D., and Kanatzidis, M.G. (2016). Rationally designing high-performance bulk thermoelectric materials. Chem. Rev. *116*, 12123–12149.

2. Ge, Z.H., Zhao, L.D., Wu, D., Liu, X., Zhang, B.P., Li, J.F., and He, J. (2016). Low-cost, abundant binary sulfides as promising thermoelectric materials. Mater. Today *19*, 227–239.

3. Zhao, L.-D., Dravid, V.P., and Kanatzidis, M.G. (2014). The panoscopic approach to high-performance thermoelectrics. Energy Environ. Sci. *7*, 251–268.

4. Xiao, Y., Wang, D., Qin, B., Wang, J., Wang, G., and Zhao, L.D. (2018). Approaching topological insulating states leads to high thermoelectric performance in n-type PbTe. J. Am. Chem. Soc. *140*, 13097–13102.

5. Wei, W., Chang, C., Yang, T., Liu, J., Tang, H., Zhang, J., Li, Y., Xu, F., Zhang, Z., Li, J.F., et al. (2018). Achieving high thermoelectric figure of merit in polycrystalline SnSe via introducing Sn vacancies. J. Am. Chem. Soc. *140*, 499–505.

6. Samanta, M., and Biswas, K. (2017). Low thermal conductivity and high thermoelectric performance in $(GeTe)_{1-2x}(GeSe)x(GeS)x$: competition between solid solution and phase separation. J. Am. Chem. Soc. *139*, 9382–9391.

7. Biswas, K., He, J., Blum, I.D., Wu, C.I., Hogan, T.P., Seidman, D.N., Dravid, V.P., and Kanatzidis, M.G. (2012). High-performance bulk thermoelectrics with all-scale hierarchical architectures. Nature *489*, 414–418.

8. Poudel, B., Hao, Q., Ma, Y., Lan, Y., Minnich, A., Yu, B., Yan, X., Wang, D., Muto, A., Vashaee, D., et al. (2008). High-thermoelectric performance of nanostructured bismuth antimony telluride bulk alloys. Science *320*, 634–638.

9. Chang, C., Wu, M., He, D., Pei, Y., Wu, C.F., Wu, X., Yu, H., Zhu, F., Wang, K., Chen, Y., et al. (2018). 3D charge and 2D phonon transports leading to high out-of-plane ZT in n-type SnSe crystals. Science *360*, 778–783.

10. Mukhopadhyay, S., Parker, D.S., Sales, B.C., Puretzky, A.A., McGuire, M.A., and Lindsay, L. (2018). Two-channel model for ultralow thermal conductivity of crystalline Tl_3e_4. Science *360*, 1455–1458.

11. Jana, M.K., Pal, K., Warankar, A., Mandal, P., Waghmare, U.V., and Biswas, K. (2017). Intrinsic rattler-induced low thermal conductivity in Zintl type $TlInTe_2$. J. Am. Chem. Soc. *139*, 4350–4353.

12. Li, B., Wang, H., Kawakita, Y., Zhang, Q., Feygenson, M., Yu, H.L., Wu, D., Ohara, K., Kikuchi, T., Shibata, K., et al. (2018). Liquid-like thermal conduction in intercalated layered crystalline solids. Nat. Mater. *17*, 226–230.

13. Jana, M.K., and Biswas, K. (2018). Crystalline solids with intrinsically low lattice thermal conductivity for thermoelectric energy conversion. ACS Energy Lett. *3*, 1315–1324.

14. Charoenphakdee, A., Yamanaka, S., and Snyder, G.J. (2008). Enhancement of thermoelectric of the electronic density of states. Science *321*, 1457–1461.

15. Zhang, Q., Liao, B., Lan, Y., Lukas, K., Liu, W., Esfarjani, K., Opeil, C., Broido, D., Chen, G., and Ren, Z. (2013). High thermoelectric performance by resonant dopant indium in nanostructured SnTe. Proc. Natl. Acad. Sci. USA *110*, 13261–13266.

16. Banik, A., Shenoy, U.S., Saha, S., Waghmare, U.V., and Biswas, K. (2016). High power factor and enhanced thermoelectric performance of $SnTe\text{-}AgInTe_2$: synergistic effect of resonance level and valence band convergence. J. Am. Chem. Soc. *138*, 13068–13075.

17. Pei, Y., Shi, X., LaLonde, A., Wang, H., Chen, L., and Snyder, G.J. (2011). Convergence of electronic bands for high-performance bulk thermoelectrics. Nature *473*, 66–69.

18. Zhao, L.D., Wu, H.J., Hao, S.Q., Wu, C.I., Zhou, X.Y., Biswas, K., He, J.Q., Hogan, T.P., Uher, C., Wolverton, C., et al. (2013). All-scale hierarchical thermoelectrics: MgTe in PbTe facilitates valence band convergence and suppresses bipolar thermal transport for high-performance. Energy Environ. Sci. *6*, 3346.

19. Rosi, F.D., Dismukes, J.P., and Hockings, E.F. (1960). Semiconductor materials for thermoelectric power generation up to 700C. Electron. Eng. *79*, 450–459.

20. Davidow, J., and Gelbstein, Y. (2013). A comparison between the mechanical and thermoelectric properties of three highly efficient p-type GeTe-Rich compositions: TAGS-80, TAGS-85 and 3%. J. Electron. Mater. *42*, 1542–1549.

21. Perumal, S., Roychowdhury, S., and Biswas, K. (2016). High-performance thermoelectric materials and devices based on GeTe. J. Mater. Chem. C *4*, 7520–7536.

22. Roychowdhury, S., Samanta, M., Perumal, S., and Biswas, K. (2018). Germanium chalcogenide thermoelectrics: electronic structure modulation and low lattice thermal conductivity. Chem. Mater. *30*, 5799–5813.

23. Chattopadhyay, T., Boucherle, J.X., and Vonschnering, H.G. (1987). Neutron diffraction study on the structural phase transition in GeTe. J. Phys. C Solid State Phys. *20*, 1431–1440.

24. Polking, M.J., Han, M.G., Yourdkhani, A., Petkov, V., Kisielowski, C.F., Volkov, V.V., Zhu, Y., Caruntu, G., Alivisatos, A.P., and Ramesh, R. (2012). Ferroelectric order in individual nanometre-scale crystals. Nat. Mater. *11*, 700–709.

25. Wu, D., Zhao, L.D., Hao, S., Jiang, Q., Zheng, F., Doak, J.W., Wu, H., Chi, H., Gelbstein, Y., Uher, C., et al. (2014). Origin of the high-performance in GeTe-based thermoelectric materials upon Bi_2Te_3 doping. J. Am. Chem. Soc. *136*, 11412–11419.

26. Perumal, S., Roychowdhury, S., Negi, D.S., Datta, R., and Biswas, K. (2015). High thermoelectric performance and enhanced mechanical stability of p-type $Ge_{1-x}Sb_xTe$. Chem. Mater. *27*, 7171–7178.

27. Perumal, S., Bellare, P., Shenoy, U.S., Waghmare, U.V., and Biswas, K. (2017). Low thermal conductivity and high thermoelectric performance in Sb and Bi codoped GeTe: complementary effect of band convergence and nanostructuring. Chem. Mater. *29*, 10426–10435.

28. Zheng, Z., Su, X., Deng, R., Stoumpos, C., Xie, H., Liu, W., Yan, Y., Hao, S., Uher, C., Wolverton, C., et al. (2018). Rhombohedral to cubic conversion of GeTe via MnTe alloying leads to ultralow thermal conductivity, electronic band convergence, and high thermoelectric performance. J. Am. Chem. Soc. *140*, 2673–2686.

29. Liu, Z., Sun, J., Mao, J., Zhu, H., Ren, W., Zhou, J., Wang, Z., Singh, D.J., Sui, J., Chu, C.W., et al. (2018). Phase-transition temperature suppression to achieve cubic GeTe and high thermoelectric performance by Bi and Mn codoping. Proc. Natl. Acad. Sci. USA *115*, 5332–5337.

30. Srinivasan, B., Gellé, A., Gucci, F., Boussard-Pledel, C., Fontaine, B., Gautier, R., Halet, J.-F., Reece, M.J., and Bureau, B. (2019). Realizing a stable high thermoelectric $zT \sim 2$ over a broad temperature range in $Ge_{1-x-y}Ga_xSb_yTe$ via band engineering and hybrid flash-SPS processing. Inorg. Chem. Front. *6*, 63–73.

31. Li, J., Zhang, X., Chen, Z., Lin, S., Li, W., Shen, J., Witting, I.T., Faghaninia, A., Chen, Y., Jain, A., et al. (2018). Low-symmetry rhombohedral GeTe thermoelectrics. Joule *2*, 976–987.

32. Roychowdhury, S., and Biswas, K. (2018). Slight symmetry reduction in thermoelectrics. Chem *4*, 939–942.

33. Wu, L., Li, X., Wang, S., Zhang, T., Yang, J., Zhang, W., Chen, L., and Yang, J. (2017). Resonant level-induced high thermoelectric response in indium-doped GeTe. NPG Asia Mater. *9*, e343–e347.

34. Hong, M., Chen, Z.G., Yang, L., Zou, Y.C., Dargusch, M.S., Wang, H., and Zou, J. (2018). Realizing zT of 2.3 in $Ge_{1-x-y}Sb_xIn_yTe$ via reducing the phase-transition temperature and introducing resonant energy doping. Adv. Mater. *30*, 1–8.

35. Gelbstein, Y., Davidow, J., Girard, S.N., Chung, D.Y., and Kanatzidis, M. (2013). Controlling metallurgical phase separation reactions of the $Ge_{0.87}Pb_{0.13}Te$ alloy for high thermoelectric performance. Adv. Energy Mater. *3*, 815–820.

36. Gelbstein, Y., and Davidow, J. (2014). Highly efficient functional $Ge_xPb_{1-x}Te$ based thermoelectric alloys. Phys. Chem. Chem. Phys. *16*, 20120–20126.

37. Fahrnbauer, F., Souchay, D., Wagner, G., and Oeckler, O. (2015). High thermoelectric figure of merit values of germanium antimony tellurides with kinetically stable cobalt germanide precipitates. J. Am. Chem. Soc. *137*, 12633–12638.

38. Perumal, S., Roychowdhury, S., and Biswas, K. (2016). Reduction of thermal conductivity through nanostructuring enhances the thermoelectric figure of merit in $Ge_{1-x}Bi_xTe$. Inorg. Chem. Front. *3*, 125–132.

39. Srinivasan, B., Boussard-Pledel, C., and Bureau, B. (2018). Thermoelectric performance of codoped (Bi, In)-GeTe and (Ag, In, Sb)-SnTe materials processed by spark plasma sintering. Mater. Lett. *230*, 191–194.

40. Li, J., Zhang, X., Lin, S., Chen, Z., and Pei, Y. (2017). Realizing the high thermoelectric performance of GeTe by Sb-doping and Se-alloying. Chem. Mater. *29*, 605–611.

41. Li, J., Chen, Z., Zhang, X., Sun, Y., Yang, J., and Pei, Y. (2017). Electronic origin of the high thermoelectric performance of GeTe among the p-type group IV monotellurides. NPG Asia Mater. *9*, e353–e358.

42. Hazan, E., Ben-Yehuda, O., Madar, N., and Gelbstein, Y. (2015). Functional graded germanium-lead chalcogenide-based thermoelectric module for renewable energy applications. Adv. Energy Mater. *5*.

43. Bohra, A.K., Bhatt, R., Singh, A., Bhattacharya, S., Basu, R., Meshram, K.N., Sarkar, S.K., Bhatt, P., Patro, P.K., Aswal, D.K., et al. (2018). Transition from n- to p-type conduction concomitant with enhancement of figure-of-merit in Pb doped bismuth telluride: material to device development. Mater. Des. *159*, 127–137.

44. Roychowdhury, S., Shenoy, U.S., Waghmare, U.V., and Biswas, K. (2017). An enhanced Seebeck coefficient and high thermoelectric performance in p-type In and Mg co-doped $Sn_{1-x}Pb_xTe$ via the co-adjuvant effect of the resonance level and heavy hole valence band. J. Mater. Chem. C *5*, 5737–5748.

45. Kim, H.S., Liu, W., Chen, G., Chu, C.W., and Ren, Z. (2015). Relationship between thermoelectric figure of merit and energy conversion efficiency. Proc. Natl. Acad. Sci. USA *112*, 8205–8210.

46. Zhao, L.D., Zhang, B.P., Li, J.F., Zhou, M., Liu, W.S., and Liu, J. (2008). Thermoelectric and mechanical properties of nano-SiC-dispersed Bi_2Te_3 fabricated by mechanical alloying and spark plasma sintering. J. Alloys Compd. *455*, 259–264.

47. Gelbstein, Y., Gotesman, G., Lishzinker, Y., Dasheky, Z., and Dariel, M.P. (2008). Mechanical properties of PbTe-based thermoelectric semiconductors. Scr. Mater. *58*, 251–254.

48. Crocker, A.J., and Wilson, M. (1978). Microhardness in PbTe and related alloys. J. Mater. Sci. *13*, 833–842.

49. Cui, J.L., Qian, X., and Zhao, X.B. (2003). Mechanical and transport properties of pseudo-binary alloys $(PbTe)_{1-x}(SnTe)_x$ by pressureless sintering. J. Alloys Compd. *358*, 228–234.

50. Darrow, M.S., White, W.B., and Roy, R. (1969). Micro-indentation hardness variation as a function of composition for polycrystalline solutions in the systems PbS/PbTe, PbSe/PbTe, and PbS/PbSe. J. Mater. Sci. *4*, 313–319.

51. Zhao, L., Wang, X., Fei, F.Y., Wang, J., Cheng, Z., Dou, S., Wang, J., and Snyder, G.J. (2015). High thermoelectric and mechanical performance in highly dense $Cu_{2-x}S$ bulks prepared by a melt-solidification technique. J. Mater. Chem. A *3*, 9432–9437.

52. Singh, A., Bhattacharya, S., Thinaharan, C., Aswal, D.K., Gupta, S.K., Yakhmi, J.V., and Bhanumurthy, K. (2009). Development of low resistance electrical contacts for thermoelectric devices based on n-type PbTe and p-type TAGS-85 $((AgSbTe_2)_{0.15}(GeTe)_{0.85})$. J. Phys. D Appl. Phys. *42*.

53. Kraemer, D., Sui, J., McEnaney, K., Zhao, H., Jie, Q., Ren, Z.F., and Chen, G. (2015). High thermoelectric conversion efficiency of MgAgSb-based material with hot-pressed contacts. Energy Environ. Sci. *8*, 1299–1308.

54. Muto, A., Yang, J., Poudel, B., Ren, Z., and Chen, G. (2013). Skutterudite unicouple characterization for energy harvesting applications. Adv. Energy Mater. *3*, 245–251.

55. Caillat, T., Firdosy, S., Li, B.C.-Y., Huang, C.-K., Cheng, B., Paik, J., Chase, J., Arakelian, T., Lara, L., and J.-P.F.. (2012). Progress status of the development of high-efficiency segmented thermoelectric couples. Nucl. Emerg. Technol. SP *3077*.

56. Salvador, J.R., Cho, J.Y., Ye, Z., Moczygemba, J.E., Thompson, A.J., Sharp, J.W., Koenig, J.D., Maloney, R., Thompson, T., Sakamoto, J., et al. (2014). Conversion efficiency of skutterudite-based thermoelectric modules. Phys. Chem. Chem. Phys. *16*, 12510–12520.

57. Caillat, T., Fleurial, J.-P., Snyder, G.J., and Borshcheky, A. (2001). Development of high efficiency segmented thermoelectric unicouples. In Proceedings ICT2001 20 International Conference on Thermoelectrics. CatTH8589) (IEEE), pp. 282–285.

58. Anatychuk, L.I., Vikhor, L.N., Strutynska, L.T., and Termena, I.S. (2011). Segmented generator modules using Bi_2Te3-based materials. J. Electron. Mater. *40*, 957–961.

59. Liu, W., Jie, Q., Kim, H.S., and Ren, Z. (2015). Current progress and future challenges in thermoelectric power generation: from materials to devices. Acta Mater. *87*, 357–376.

60. Aoyama, I., Kaibe, H., Rauscher, L., Kanda, T., Mukoujima, M., Sano, S., and Tsuji, T. (2005). Doping effects on thermoelectric properties of higher manganese silicides (HMSs, $MnSi_{1.74}$) and characterization of thermoelectric generating module using p -type (Al, Ge and Mo)-doped HMSs and n -Type $Mg_2Si_{0.4}Sn_{0.6}$ legs. Jpn. J. Appl. Phys. *44*, 4275–4281.

61. Groß, E., Riffel, M., and Stöhrer, U. (1995). Thermoelectric generators made of $FeSi_2$ and HMS: fabrication and measurement. J. Mater. Res. *10*, 34–40.

62. Jood, P., Ohta, M., Yamamoto, A., and Kanatzidis, M.G. (2018). Excessively doped PbTe with Ge-induced nanostructures enables high-efficiency thermoelectric modules. Joule *2*, 1339–1355.

63. Chetty, R., Kikuchi, Y., Bouyrie, Y., Jood, P., Yamamoto, A., Suekuni, K., and Ohta, M. (2019). Power generation from the $Cu_{26}Nb_2Ge_6S_{32}$-based single thermoelectric element with Au diffusion barrier. J. Mater. Chem. C *7*, 5184–5192.

64. Zong, P., Hanus, R., Dylla, M., Tang, Y., Liao, J., Zhang, Q., Snyder, G.J., and Chen, L. (2017). Skutterudite with graphene-modified grain-boundary complexion enhances zT enabling high-efficiency thermoelectric device. Energy Environ. Sci. *10*, 183–191.

65. Zhang, Q., Liao, J., Tang, Y., Gu, M., Ming, C., Qiu, P., Bai, S., Shi, X., Uher, C., and Chen, L. (2017). Realizing a thermoelectric conversion efficiency of 12% in bismuth telluride/skutterudite segmented modules through full-parameter optimization and energy-loss minimized integration. Energy Environ. Sci. *10*, 956–963.